J Mater Sci (2009) 44:2700–2704
DOI 10.1007/s10853-009-3354-6

Amorphous Ti–Cu–Ni–Al alloys prepared by mechanical alloying

Hoang-Viet Nguyen · Ji-Soon Kim · Young-Soon Kwon · Jin-Chun Kim

Received: 3 December 2008 / Accepted: 17 February 2009 / Published online: 13 March 2009

Abstract $Ti_x(CuNi)_{90-x}Al_{10}$ ($x = 50$, 55, 60) amorphous powder alloys were synthesized by mechanical alloying technique. The evolution of amorphization during milling and subsequent heat treatment was investigated by scanning electron microscopy, X-ray diffraction, differential scanning calorimetry and transmission electron microscopy. The fully amorphous powders were obtained in the $Ti_{50}Cu_{20}Ni_{20}Al_{10}$, $Ti_{55}Cu_{17.5}Ni_{17.5}Al_{10}$ and $Ti_{60}Cu_{15}Ni_{15}Al_{10}$ alloys after milling for 30, 20 and 15 h, respectively. Differential scanning calorimetry revealed that thermal stability increased with the increasing (CuNi) content: $Ti_{60}Cu_{15}Ni_{15}Al_{10}$, $Ti_{55}Cu_{17.5}Ni_{17.5}Al_{10}$ and $Ti_{50}Cu_{20}Ni_{20}Al_{10}$. Heating of the three amorphous alloys at 800 K for 10 min results in the formation of the NiTi, $NiTi_2$ and $CuTi_2$ intermetallic phases.

Introduction

Ti-based bulk metallic glasses (BMG) are regarded as highly promising engineered materials for expanding the possible applications of bulk amorphous materials due to their light-weight, outstanding mechanical properties, and excellent corrosion resistance [1]. Amorphization of alloys is thought to cause a remarkable increase in mechanical strength and corrosion resistance; consequently, a number of studies on the amorphization of Ti-based alloys have been carried out. It has been reported that amorphous materials containing Ti as the main constituent element have been produced by melt spinning [2–5] in various systems such as Ti–Ni–Cu, Ti–Nb–Si–B, Ti–Ni–Cu–Al, Ti–Zr–Ni–Cu–Al and Cu–Ti–Zr–Al. However, it has been difficult to prepare the Ti–Cu-based BMGs of a large size. The maximum size of samples produced by rapid quenching techniques is only of the order of few millimeters for as-cast Ti-based systems [6]. To overcome the size and shape limitations of BMGs, there have been some attempts carried out to produce bulk amorphous alloys by powder metallurgy processing [7, 8]. Mechanical alloying (MA) has proven to be an effective and relatively simple method of producing amorphous powder materials [9–13]. The as-milled powder alloys are suitable for further processing; for example, bulk amorphous $Ti_{50}Cu_{25}Ni_{20}Sn_5$ [14] and Al–La–Ni–Fe [15] alloys were consolidated by spark-plasma sintering of mechanically alloyed $Ti_{50}Cu_{25}Ni_{20}Sn_5$ and $Al_{82}La_{10}Ni_4Fe_4$ powders, respectively.

This paper focuses on the mechanically alloyed systems of $Ti_x(CuNi)_{90-x}Al_{10}$ ($x = 50$, 55, 60) compositions. The amorphous powder alloys were synthesized by MA. Phase transformation, thermal stability and crystallization behavior of the mechanically alloyed amorphous powders were investigated.

Experimental

The elemental powders of Ti, Cu, Ni and Al with purity greater than 99% were mixed in proportions corresponding to the compositions of $Ti_x(CuNi)_{90-x}Al_{10}$, $x = 50$, 55, 60. MA was performed using an AGO-2 planetary ball mill with a speed of 300 rpm. Hardened steel vials and balls were used, and the ball-to-powder weight ratio was 20:1. The vials were evacuated and filled with 5×10^3 Pa Ar gas to avoid oxidation of the powder particles. During milling,

H.-V. Nguyen · J.-S. Kim · Y.-S. Kwon · J.-C. Kim (✉)
Research Center for Machine Parts and Materials Processing, School of Materials Science and Engineering, University of Ulsan, Namgu Mugeo 2-Dong, San 29, Ulsan 680-749, Korea
e-mail: jckimpml@ulsan.ac.kr

the vials were cooled by water in order to prevent an increase in temperature. The MA process was carried out using selected time durations from 1 to 30 h. Each MA process was performed without interruptions. X-ray diffraction (XRD) using Cu-K_α radiation of 1.54178 Å was used for analysis of the phase formation in the milled powder samples. Morphology of the mechanically alloyed powder samples was observed by a JEOL JMS-6500F field emission scanning electron microscope (FE-SEM). Transmission electron microscopy (TEM) observation was carried out in a TEM/STEM/EDS Tecnai 20-EDS Phoenix microscope. Thermal properties of the as-milled amorphous powders were evaluated by differential scanning calorimetry (DSC) with a heating rate of 10 K/min under a continuous flow of Ar gas.

Results and discussion

Although amorphous alloys could be synthesized for all compositions investigated in the present work, $Ti_{50}Cu_{20}Ni_{20}Al_{10}$ composition was chosen as a model and investigated in detail. The FE-SEM images of the cross-sections of the powder of the $Ti_{50}Cu_{20}Ni_{20}Al_{10}$ alloy as a function of milling time are shown in Fig. 1. The composite powder particle with many intimately contacting layers of the elemental metals can be seen in the micrograph in Fig. 1a and b. The lamellar thickness decreased gradually with increasing milling time. The lamellar layers became undistinguishable after milling for 10 and 30 h. In addition, the microstructure changed significantly and a fine structure was evident (Fig. 1c–d). The result indicates enhanced diffusion of the elemental metals and the onset of the solid-state amorphization reaction.

The evolution of amorphization during milling process was monitored by means of XRD. The XRD patterns of $Ti_{50}Cu_{30}Ni_{20}Al_{10}$ powders after milling times ranging from 1 to 30 h are shown Fig. 2. The bottom curve shows the XRD pattern of the powder mixture after 1 h of milling. The most intense peaks corresponding to crystalline Ti, Cu, Ni and Al elements are indexed in the pattern. A continuous decrease in intensity and broadening of the metal peaks are evident with increasing milling time as seen from Fig. 2a–c. After milling for 2 and 5 h, the intensity of the crystalline Ti, Cu, Ni and Al peaks decreased and a broad peak corresponding to the amorphous phase appeared. After 10 and 20 h of milling, traces of the crystalline Cu, Ni and Al peaks vanished simultaneously. When the milling time was extended, the broadening of the diffuse diffraction maximum was not observed anymore. Within 10–30 h of milling, the position of the diffuse diffraction saturated at around $2\theta = 41.7°$. It indicates that the milling process leads to enhancement of the chemical homogeneity in the alloyed amorphous phase until a steady state of the structural evolution is achieved [16]. After 30 h of milling, the elemental powder mixture was transformed completely

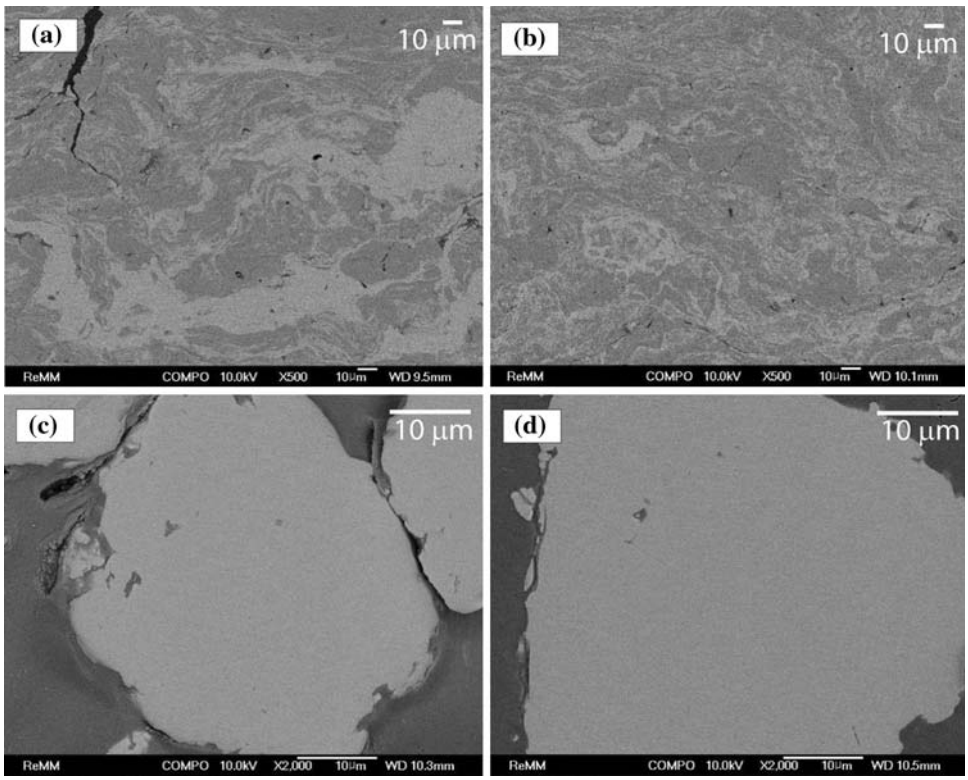

Fig. 1 Back-scattering electron SEM images of cross-sections of $Ti_{50}Cu_{20}Ni_{20}Al_{10}$ powders milled for **a** 2 h, **b** 5 h, **c** 10 h and **d** 30 h

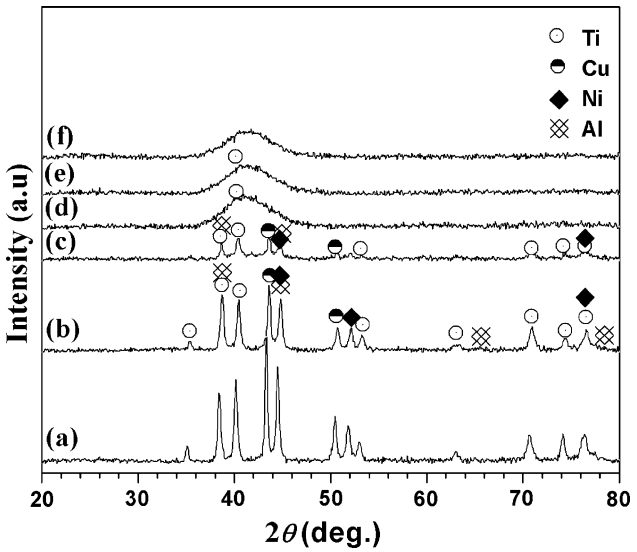

Fig. 2 XRD patterns of $Ti_{50}Cu_{20}Ni_{20}Al_{10}$ powder alloy milled for (a) 1 h, (b) 2 h, (c) 5 h, (d) 10 h, (e) 20 h and (f) 30 h

into a fully amorphous $Ti_{50}Cu_{30}Ni_{20}Al_{10}$ alloy. No diffraction peaks of any crystalline metallic phases or oxides were observed.

The high-resolution transmission electron micrograph (HR-TEM) and the corresponding electron diffraction pattern of the $Ti_{50}Cu_{20}Ni_{20}Al_{10}$ powder alloy after milling for 30 h is given in Fig. 3. A selected area diffraction pattern (SADP) taken from this region shows a diffuse halo ring indicating the formation of the amorphous phase.

Figure 4a–f shows the XRD patterns of the $Ti_{55}Cu_{17.5}Ni_{17.5}Al_{10}$ alloy powder after different milling durations. At the early stage of milling (1 h), the crystalline Ti, Cu, Ni and Al peaks were detected. The peak intensity of the crystalline Ti, Cu, Ni and Al decreased significantly after 2 h of milling. A broad halo corresponding to the amorphous phase was superimposed on the Ti major diffraction peak at around $2\theta = 40.2°$ after 5 h of milling. The traces of crystalline Ti are still detected along with the amorphous phase after milling for 15 h (Fig. 4e). The fully amorphous $Ti_{55}Cu_{17.5}Ni_{17.5}Al_{10}$ alloy was obtained after milling of 20 h.

Similarly, the XRD patterns of the $Ti_{60}Cu_{15}Ni_{15}Al_{10}$ alloy powders are shown in Fig. 5. After 5 h of milling, XRD pattern shows a halo corresponding to the amorphous phase and only the peaks of elemental Ti were observed. The fully amorphous alloy can be obtained in the $Ti_{60}Cu_{15}Ni_{15}Al_{10}$

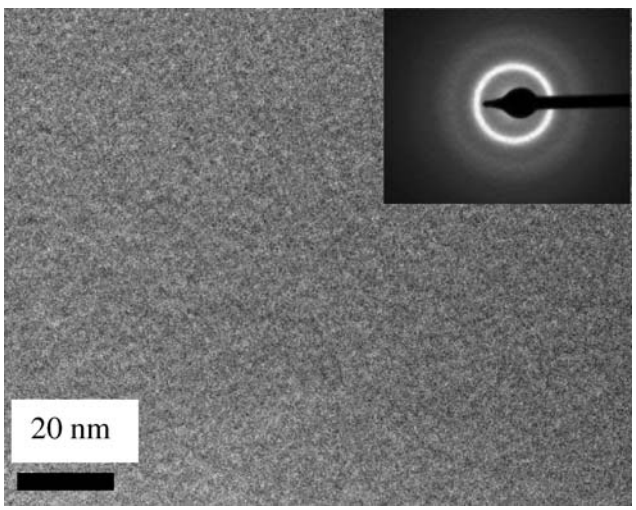

Fig. 3 HR-TEM micrograph (*inset*: selected area diffraction pattern) of the $Ti_{50}Cu_{20}Ni_{20}Al_{10}$ powder alloy milled for 30 h

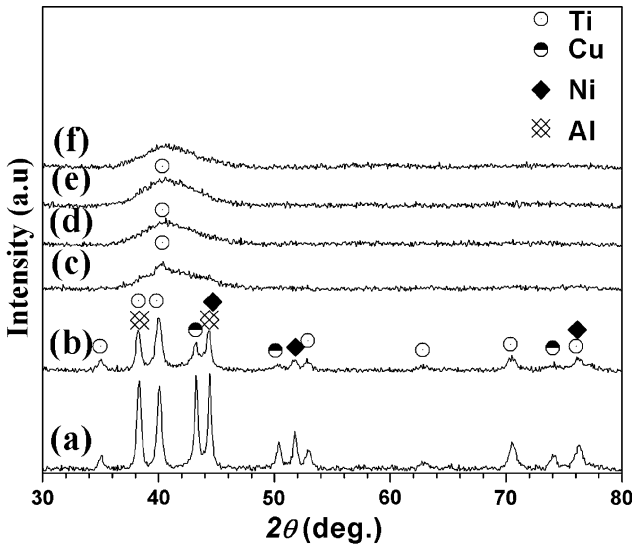

Fig. 4 XRD patterns of the $Ti_{55}Cu_{17.5}Ni_{17.5}Al_{10}$ powder milled for (a) 1 h, (b) 2 h, (c) 5 h, (d) 10 h, (e) 15 h and (f) 20 h

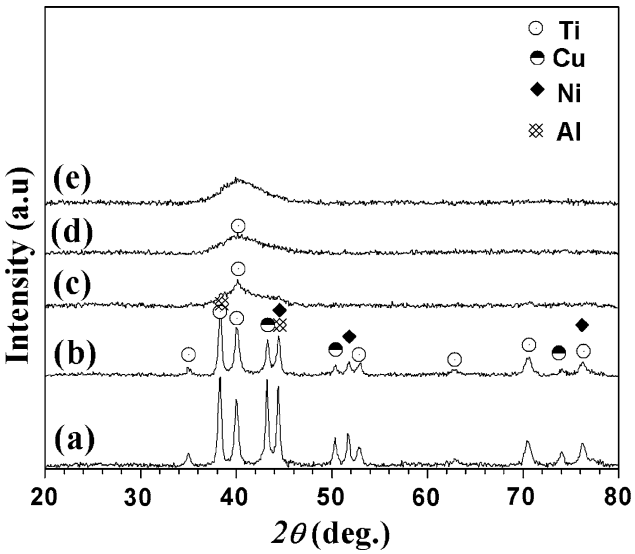

Fig. 5 XRD patterns of $Ti_{60}Cu_{15}Ni_{15}Al_{10}$ powder milled for (a) 1 h, (b) 2 h, (c) 5 h, (d) 10 h and (e) 15 h

system after milling for 15 h. The amorphous halos of the $Ti_{50}Cu_{20}Ni_{20}Al_{10}$, $Ti_{55}Cu_{17.5}Ni_{17.5}Al_{10}$ and $Ti_{60}Cu_{15}Ni_{15}Al_{10}$ alloys have their maxima located at a wave number of $k = \frac{4\pi \sin\theta}{\lambda}$ of 29.0, 28.5 and 28.2 nm^{-1}, respectively. The shift of the maximum of the amorphous halo with the (CuNi) content is in agreement with the observation made for Ti–Ni–Cu system by Murty et al. [17]. The shift of the maximum of the amorphous halo to a higher value of the wave number with increasing (CuNi) content indicates a decrease in the nearest neighbor distance due to the formation of a greater number of the Cu-pairs and Ni-pairs [17].

The milling time required for amorphization in the $Ti_{50}Cu_{20}Ni_{20}Al_{10}$, $Ti_{55}Cu_{17.5}Ni_{17.5}Al_{10}$ and $Ti_{60}Cu_{15}Ni_{15}Al_{10}$ alloys is 30, 20 and 15 h, respectively, i.e., it decreases with decreasing (CuNi) content and increasing Ti content. Ti has a high solubility of Al without formation of an intermetallic compound; however, Ni and Cu have a limited solubility of Al [18, 19]. The limited solubility of Al in both Ni and Cu promotes the formation of intermetallic compounds and hence hinders the formation of the amorphous phase. Similar observations regarding the glass-forming ability of melt-spun equiatomic (Ti, Zr, Hf, Nb)–(Ni, Cu, Ag)–Al alloys were made by Kim et al. [20].

Figure 6 shows the DSC traces of the $Ti_x(CuNi)_{90-x}Al_{10}$ ($x = 50$, 55 and 60) after milling for 30 h. The DSC curves exhibit an endothermic event characteristic of the glass transition, followed by a supercooled liquid region (SLR) $\Delta T_x = T_x - T_g$ and crystallization. The crystallization in the $Ti_{50}Cu_{20}Ni_{20}Al_{10}$ alloy proceeded in one stage while in the $Ti_{60}Cu_{15}Ni_{15}Al_{10}$ and $Ti_{55}Cu_{17.5}Ni_{17.5}Al_{10}$ alloys it occurred in three stages. The DSC curves of the $Ti_{55}Cu_{17.5}Ni_{17.5}Al_{10}$ and $Ti_{60}Cu_{15}Ni_{15}Al_{10}$ amorphous alloys are similar to those of the melt-spun samples of $(TiZrHf)_x(CuNiCo)_{90-x}Al_{10}$. Then, the large exothermic event corresponds to the crystallization

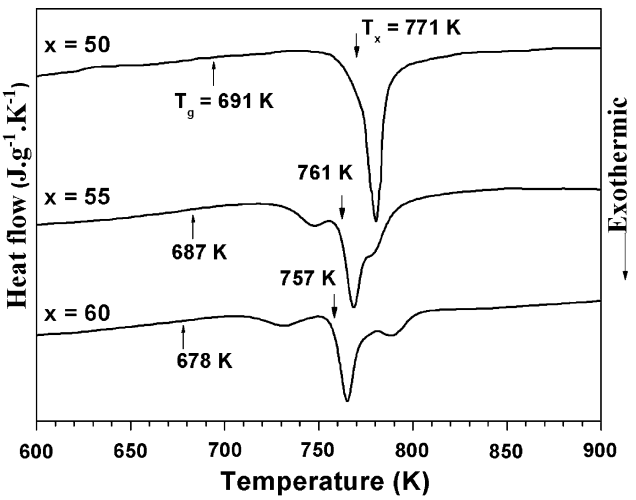

Fig. 6 DSC traces of the $Ti_x(CuNi)_{90-x}Al_{10}$ amorphous powders after milling for 30 h (heating rate of 10 K min^{-1})

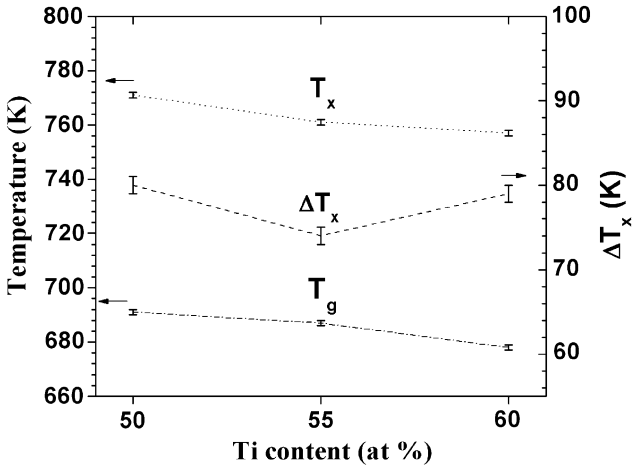

Fig. 7 Glass transition temperature, T_g, onset temperature of crystallization, T_x, and supercooled liquid region, ΔT_x, obtained from the DSC scans for the alloy $Ti_x(CuNi)_{90-x}Al_{10}$ as function of Ti content

of the amorphous phase leading to the mixture of intermetallics AlCuHf and Ti_2Cu_3 after heating above the temperature of the second crystallization peak [21].

The glass transition temperatures, onset temperatures of the crystallization and the width of the supercooled liquid region of the alloys are plotted in Fig. 7. As the Ti content increases and the (NiCu) content decreases, both the T_g and T_x gradually shift to lower temperatures. T_g and T_x move from 691 and 771 K for $x = 50$ to 678 and 757 K for $x = 60$, respectively. A similar trend of T_g and T_x was observed by Zhang as the Ti content increased from 50 to 60 at.% in the mechanically alloyed $(TiZrNb)_x(CuNiCo)_{90-x}Al_{10}$ powders [22].

To identify the structural changes related to the crystallization event, the powders were heated in the DSC to 800 K with a heating rate of 20 K/min, held for 10 min and then cooled down to room temperature for the subsequent XRD measurements. Heating of the three amorphous alloys results in the formation of NiTi, $NiTi_2$ and $CuTi_2$ intermetallic phases as seen in Fig. 8. For the amorphous powder of the $Ti_{50}Cu_{20}Ni_{20}Al_{10}$ system, a small volume fraction of $CuTi_2$ phase was found along with the $NiTi_2$ and NiTi phases. The volume fractions of the $NiTi_2$ and $CuTi_2$ phases increase with increasing Ti content from 50 to 60 at.%, while the volume fraction of the NiTi phase decreases significantly.

Conclusions

$Ti_x(CuNi)_{90-x}Al_{10}$ ($x = 50$, 55, 60) amorphous powder alloys have been successfully synthesized by mechanical alloying. The fully amorphous structure could be obtained in $Ti_x(CuNi)_{90-x}Al_{10}$ alloys with the Ti content of 50, 55

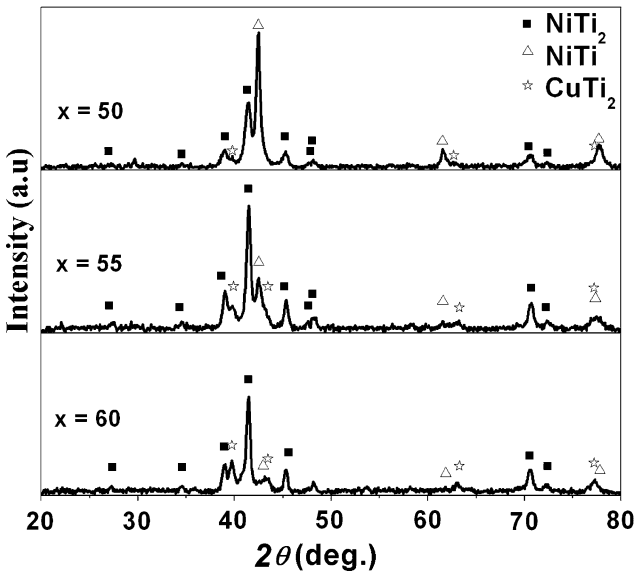

Fig. 8 Crystalline phases of the $Ti_x(CuNi)_{90-x}Al_{10}$ amorphous powders after heat treatment at 800 K for 10 min

and 60 at.% after 30, 20 and 15 h, respectively. The $Ti_{50}Cu_{20}Ni_{20}Al_{10}$ alloy exhibited the highest thermal stability and the largest supercooled liquid region of 80 K among the three alloys. The results of this study are promising for the development of the Ti–Cu–Ni–Al amorphous alloys by powder metallurgy processing and the amorphous powder alloys with large SLR ΔT_x values (>74 K), which is beneficial for the consolidation of mechanically alloyed powders.

Acknowledgement This work was financially supported by the 2006 Research Fund of Korean Research Foundation (MOHARD) (KRF-2006-2110D00221).

References

1. Kim YC, Kim WT, Kim DH (2004) Mater Sci Eng A 375–377:127
2. Zhang T, Inoue A (1998) Mater Trans JIM 39:1001
3. Inoue A, Nishiyama N, Amiya K, Zhang T, Masumoto T (1994) Mater Lett 19:131
4. Amiya K, Nishiyama N, Inoue A, Masumoto T (1994) Mater Sci Eng A 179–180:692
5. Inoue A (1999) Mater Sci Forum 312–314:307
6. Louzguine DV, Inoue A (2000) Scr Mater 43:371
7. Hiromichi F, Victoria AY, Takashi M, Sadahiro T (2008) J Mater Sci 43:3837. doi:10.1007/s10853-007-2220-7
8. Lin HM, Lin YW, Lee PY (2008) J Mater Sci 43:3118. doi:10.1007/s10853-008-2504-6
9. Amini R, Hadianfard MJ, Salahinejad E, Marasi M, Sritharan T (2009) J Mater Sci 44:136. doi:10.1007/s10853-008-3117-9
10. Weeber AW, Bakker H (1988) Physica B 153:93
11. Koch CC, Cavin OB, McKamey CG, Scarbrough JO (1983) Appl Phys Lett 43:1017
12. El-Eskandarany MS, Aoki K, Suzuki K (1990) J Less-Common Met 167:113
13. Kim TS, Lee JK, Kim HJ, Bae JC (2005) Mater Sci Eng A 402:228
14. Choi PP, Kim JS, Nguyen OTH, Kwon YS (2007) J Mater Lett 61:4591
15. Choi PP, Kim JS, Nguyen OTH, Kwon YS (2007) Mater Sci Eng A 449–451:1119
16. Zhang LC, Xu J (2002) J Mater Lett 56:615
17. Murty S, Rao SM, Ranganathan S (1990) Scr Metall 24:1819
18. Massalski TB (1990) Binary alloy phase diagram. ASM International, Materials Park, OH
19. Villars P, Prince A, Okamoto H (1995) Handbook of ternary alloy phase diagram. ASM International, Materials Park, OH
20. Kim KB, Warren PJ, Cantor B (2003) J Non-Cryst Solids 317 (1–2):17
21. Zhang LC, Xu J (2004) J Non-Cryst Solids 347:166
22. Zhang LC, Kim KB, Yu P, Zhang WY, Kunz U, Eckert J (2007) J Alloys Compd 428:157